Available online at www.sciencedirect.com

ScienceDirect

journal homepage: www.elsevier.com/locate/he

Increasing energy efficiency of hydrogen refueling stations via optimal thermodynamic paths

Diego F. Mendoza [a,*], *David Rincon* [b], *Bruno F. Santoro* [c]

[a] *Department of Chemical Engineering, Universidad de Antioquia, Calle 70 No. 52 - 21, Medellin, 050010, Antioquia, Colombia*

[b] *Department of Chemical and Biomolecular Engineering, University of California, 5531 Boelter Hall, Los Angeles, 90095-1592, CA, USA*

[c] *Op2B - Optimization to Business, Av. Pompeia, 723, Sao Paulo, 05023-000, SP, Brazil*

HIGHLIGHTS

- A dynamic model of a hydrogen refueling station (HRS) is derived and validated.
- HRS irreversibilities during the refueling are quantified via entropy production.
- Energy savings of 27% using a minimal entropy production strategy over SAE J2601.
- Sensitivity of results is checked for outside temperature and model parameters.
- Under near-reversible conditions, energy savings were 43% with respect to SAE J2601.

GRAPHICAL ABSTRACT

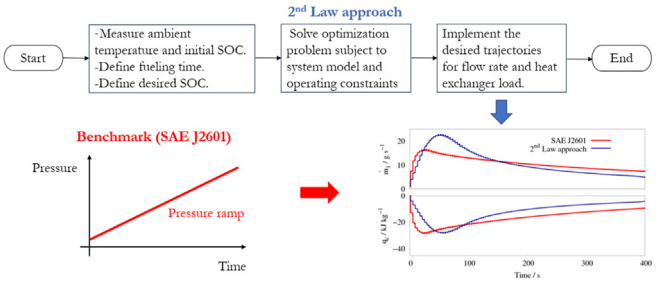

ARTICLE INFO

Article history:
Received 8 July 2023
Received in revised form
30 August 2023
Accepted 3 September 2023
Available online 23 September 2023

Keywords:
Energy efficiency
Entropy production
Optimal control

ABSTRACT

This work addresses the energy efficiency of hydrogen refueling stations (HRS) using a first-principles model and optimal control methods to find minimal entropy production operating paths. The HRS model shows good agreement with experimental data, achieving maximum state of charge and temperature discrepancies of 1 and 7%, respectively. Model solution and optimization is achieved at a relatively low computational time (40 s) when compared to models of the same degree of accuracy. The entropy production mapping indicates the flow control valve as the main source of irreversibility, accounting for 85% of the total entropy production in the process. The minimal entropy production refueling path achieves energy savings from 20 to 27% with respect to the SAE J2601 protocol, depending on the ambient temperature. Finally, the proposed method under near-reversible refueling conditions shows a theoretical reduction of 43% in the energy demand with respect to the SAE J2601 protocol.

* *Corresponding author.*
E-mail address: dfernando.mendoza@udea.edu.co (D.F. Mendoza).

https://doi.org/10.1016/j.ijhydene.2023.09.027

Hydrogen refueling station
SAE J2601

Nomenclature

Latin

A	Area, m^2
a	Helmholtz equation parameter
b	Helmholtz equation parameter
D	Helmholtz equation parameter
$\mathcal{K}$	Index
k	Valve flow capacity coefficient, $m^3\ h^{-1}$
h	Heat transfer coefficient, kW $m^{-2}\ K^{-1}$
$\dot{m}(t)$	Mass flow rate, kg s^{-1}
$p(t)$	Pressure, kPa
p_c	Critical pressure, kPa
ps	Pipe segment,
$q(t)$	Specific heat flow, kJ kg^{-1}
R	Ideal gas constant, kJ $kg^{-1}\ K^{-1}$
$S(t)$	Entropy, kJ K^{-1}
$S_{irr}(t)$	Total entropy production, kJ K^{-1}
$s(t)$	Specific entropy, kJ $kg^{-1}\ K^{-1}$
$T(t)$	Temperature, K
t	Time, s
t_i	Helmholtz equation parameter,
T_c	Critical temperature, K
$u(t)$	Specific internal energy, kJ kg^{-1}
V	Vehicle tank volume, m^3

Greek

α	Helmholtz equation parameter
δ	Helmholtz equation parameter
γ	Helmholtz equation parameter
φ	Helmholtz equation parameter
$\rho(t)$	Density, kg m^{-3}
ρ_N	Density at normal conditions (273.15 K, 101.325 kPa), kg m^{-3}
ρ_c	Critical density, kg m^{-3}
ρ_{full}	Maximum admissible density in the vehicle tank kg m^{-3}
τ	Helmholtz equation parameter

Subscripts

f	Final
fv	Flow control valve
i	Index
iv	Inlet valve
irr	Irreversible
k	Index
w	Wall
0	Tank
32	Pipe segment 32
54	Pipe segment 54
∞	Ambient

Superscripts

0	Ideal gas
r	Residual
ref	Reference state
k	Index

1. Introduction

In order to be viable and attractive to the market, hydrogen fuel cell electric vehicles (FCEVs) rely on the proper coordination of multiple factors such as safety operation, user experience, vehicle cost, and location. Hydrogen technologies have been explored in different scenarios. For example, multi energy systems (i.e, electricity, hydrogen, and heat) have increased their resilience [1]. Specifically in terms of transport, there is an economic study about supplying the taxi fleet with hydrogen instead of from hydrocarbon fuels in the city of Rabat, Morocco, suggesting that economies of scale are present in this transition [2]. Energy performance and fueling events of hydrogen refueling stations have been studied with real refueling data from the Cal State LA Hydrogen Research and Fueling Facility from 2016 to 2020 in which it is recommended more attention to optimizing equipment energy expenditure [3,4].

Hydrogen refueling stations (HRSs) availability and cost are considered critical for a successful insertion of FCEVs in the market [5–7]. Regarding user experience, the fueling protocol SAE J2601 has been designed to approach the hydrogen filling time of the combustion engine vehicles. However, SAE J2601 is a lookup table in its simpler form that defines the average pressure ramp rate based on ambient temperature and the tank's initial pressure, without adjustments that a feedback controller can provide. For the fueling station efficiency, most contributions in the literature are based on analyses focused on the first law of thermodynamics.

Design, analysis and optimization of the refueling process in HRSs have been approached using process systems engineering techniques and thermodynamic methods. For instance, a model based on thermodynamics and transport phenomena has been validated with experimental data to simulate the fill-up process of FCEVs [8]. Due to the maximum temperature limit inside the vehicle tank and in order to improve the user experience, an optimal control strategy has been proposed to minimize the fill-up time [9]. A thermodynamic analysis is performed for the refueling process of a tank under different equations of state, in which the ideal-gas assumption shows under-estimation of temperature and

pressure for hydrogen [10]. Computational fluid dynamics (CFD) was implemented to identify the main conditions that ensure gas temperature homogeneity in the tank during the hydrogen refueling process [11]. By means of dynamic simulations, the design of hydrogen refueling stations was optimized, reducing energy demand and compressor power consumption [12]. A thermodynamic-based model for a hydrogen refueling station has been proposed by considering heat transfer from the tanks, pressure loses in the system, cooling demands, and compressor work, in which the number of tanks at different pressure levels in the station and conditions were evaluated [13]. Similarly, the economical benefits of HRSs using cascade design for buses is shown over the single-tank configuration [14]. Entropy production was reduced by 55% when comparing to a cascade storage (i.e., three vessels) and a buffer (i.e., one vessel) hydrogen fuelling station based on open-loop simulations [15]. The impact of pipelines on cooling demand in HRSs has been estimated on 9.9% [16]. In a recent review for hydrogen refueling stations, it was pointed out the urgency for more studies that target cost minimization and maximization of equipment efficiency by means of optimization of their parameter design and quantity configuration [17]. Still, little attention has been paid to optimize the entropy production of hydrogen fueling stations [17,18].

To enhance the user experience while filling hydrogen vehicle and maintaining the integrity of the storage system, SAE J2601 was introduced as a standard for refueling stations in 2014 [19,20]. SAE J2601 proposes two different methods, one based on a lookup table and the MC formula [21,22]. In contrast to the lookup table, the MC formula-based method only outperforms the simpler alternative in fueling time under some conditions, but this result is achieved by using 6.9% more energy [21,23]. An optimization framework was proposed to calculate the pressure switching coefficient and precooling temperature of hydrogen in a cascade storage system of a hydrogen filling process by targeting faster refueling, lower energy consumption and higher state of charge (SOC) [24]. Simulations showed higher SOC can be obtained with the implemented lumped parameter thermodynamic model based on the first law [24].

Based on the above, this paper proposes an optimal control algorithm for the fill-up process of FCEVs based on the minimization of entropy production. To our knowledge, current protocols for hydrogen refueling stations only explicitly take into account the first law of thermodynamics. In this regard, the main contributions of this paper are:

- The determination of minimum entropy production paths for refueling operations in hydrogen stations using a rigorous mathematical model and dynamic optimization tools.
- The identification of operating conditions that could improve the energy efficiency over the SAE J2601 protocol.
- The proposal of a thermodynamic efficiency limit for hydrogen refueling stations defining a near-reversible operation.

The model is first validated with experimental data to check its predictions. Then, the optimization algorithm is evaluated and compared with the SAE J2601 protocol under different realistic scenarios. Finally, the simulation conditions are modified in order to mimic a near-reversible process with the intent of finding a lower bound of entropy production for further practical applications. This work establishes an entropy production based model to investigate the benefits of finding different process paths that minimize energy consumption by avoiding, for example, fixed pressure ramps.

2. Methodology

2.1. *Refueling station layout*

Typical HRS layout consists of compressors, storage tanks, cooling units, valves and dispensers [7]. In this contribution, it is of interest working with a simplified HRS topology with the purpose of illustrating how entropy production minimization provides the thermodynamic optimal operation of HRS and how this optimal condition can be used to identify possible improvements in the energy efficiency of the current SAE J2601 protocol defined by the lookup table using a H70-T40 dispenser.

The simplified refueling station to be modeled and optimized (see Fig. 1) consists of a high pressure hydrogen stream from the supply tanks (Stream 6) whose flow is regulated by the control valve. The isenthalpic expansion in the valve causes a temperature rise in the outlet stream (Stream 5), which can be detrimental for the operation safety, as well as for the final SOC achieved in the vehicle tank. For this reason, a cooler is placed after the flow control valve to regulate the hydrogen temperature delivered into the vehicle tank (Stream 3). Finally, the pressure and thermally conditioned hydrogen (Stream 2) is dispensed into the vehicle tank through the inlet valve.

2.2. *Mathematical modeling*

The mathematical model of the HRS is a modification of the model presented in Ref. [8]. The main differences introduced in this work consist in using a high accuracy thermodynamic model, a better description of the valves, and entropy balances. The refueling model takes into account each component shown in Fig. 1, namely, the flow control and tank inlet valves, the cooler and the vehicle tank, including its wall. Each component is described by the mass and energy balances, as well as by the constitutive equations for heat transfer in the tank, pressure drop in valves, internal energy, entropy, and pressure–density–temperature relationships for the thermodynamic description of hydrogen in each part of the process.

2.2.1. *Model assumptions*

The model is aimed at capturing the main thermal characteristics during the refueling process at reasonable computational cost, envisaging real time applications. The main assumptions are: (i) uniform temperature and pressure of hydrogen inside the vehicle tank, (ii) uniform tank-wall temperature, (iii) instantaneous steady state in valves, pipes and cooler, (iv) negligible pressure drop in pipes and cooler, and (v) adiabatic pipes and valves.

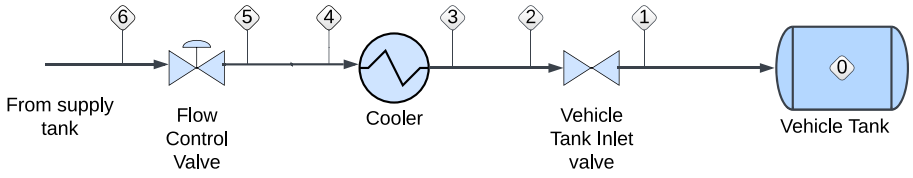

Fig. 1 – Hydrogen station layout.

The first Assumption is supported by experiments and CFD simulations for cases where the nozzle in the vehicle tank allows a uniform expansion of hydrogen during the filling process [25,26].

Regarding Assumption (ii), thermal dynamics of the tank wall has been modeled using two main approaches. The first one (distributed-parameter approach) applies the transient heat conduction equation to obtain the spatial temperature distribution in the wall during the filling process [11,12,27]. The second one (lumped-parameter approach) neglects the spatial variation of temperature, taking into account the time variation of a representative wall temperature [8]. In principle, the distributed-parameter approach would allow better calculation of the heat transfer rate between the hydrogen and the tank wall than the lumped-parameter approach, but the degree of uncertainty on the true value of the heat transfer coefficient during the filling process does not confer a real advantage of the distributed-parameter over the lumped-parameter approach [28]. On the other hand, the significant computational cost reduction by using the lumped-parameter approach favors it in this work.

Assumption (iii) is supported by the relatively negligible volume of valves, pipe segments and cooler, compared to the vehicle tank capacity, which anticipates a fast dynamics in all components of the HRS, except in the vehicle tank [8,12].

In most cases the operation conditions in the refueling stations are such that hydrogen flow can be described according to the incompressible fluid model [8]. Under this circumstance, pressure drops in the cooler and pipe segments tend to be negligible compared to the pressure drop in valves [8], as expressed by Assumption (iv).

Finally, the adiabatic flow in pipes and valves stated in Assumption (v) is achieved if the refueling station is designed with a well-insulated pipe network.

2.2.2. *Model equations*

Model equations are presented for each process component, corresponding to the vehicle tank, valves, cooler and pipes. The complete list of time-dependent variables and model parameters is provided in the Nomenclature section. However, in the following equations, time-dependencies are omitted for ease of reading.

2.2.2.1. Vehicle tank. The mass and energy balances of the hydrogen inside the tank, Eqs. (1) and (2), take into account density, ρ_0, and internal energy dynamics, u_0, assuming mass and energy interactions with the inlet stream and the tank wall:

$$V_0\frac{d\rho_0}{dt} = \dot{m}_1 \tag{1}$$

$$V_0\rho_0\frac{du_0}{dt} = \dot{m}_1\left(u_1 - u_0 + \frac{p_1}{\rho_1}\right) + h_{w0}A_{w0}(T_0 - T_w) \tag{2}$$

$$p_0 = p_0(T_0, \rho_0) \tag{3}$$

$$p_1 = p_1(T_1, \rho_1) \tag{4}$$

$$u_0 = u_0(T_0, \rho_0) \tag{5}$$

$$u_1 = u_1(T_1, \rho_1) \tag{6}$$

where V_0 is the tank volume, h_{w0} is the heat transfer coefficient between the gas and the wall, A_{w0} is the tank internal wall area; T_0, p_0 are the hydrogen temperature and pressure in the tank; $\dot{m}_1$, u_1 and p_1 are the mass flow rate, specific internal energy and pressure of the tank inlet stream, respectively. Further, it is assumed that inlet stream and vehicle-tank pressures are the same during the refueling process:

$$p_0 = p_1 \tag{7}$$

The SOC is a useful indicator to characterize a complete fill. It is defined as the ratio of the actual hydrogen density in the vehicle tank, ρ_0, with respect to a reference density, ρ_{full}, corresponding to the hydrogen density at the service pressure at 15 °C [29],

$$SOC = \frac{\rho_0}{\rho_{full}} \tag{8}$$

The tank-wall thermal dynamics is represented by a lumped-parameter energy balance across the tank wall:

$$\rho_w V_w c_{pw}\frac{dT_w}{dt} = h_{w0}A_{w0}(T_0 - T_w) - h_{w\infty}A_{w\infty}(T_w - T_\infty) \tag{9}$$

where T_w is the wall temperature, $h_{w\infty}$ is the wall-ambient heat transfer coefficient, T_∞ is the ambient temperature, $A_{w\infty}$ is the external area of the tank wall, ρ_w, V_w and c_{pw} denote density, volume and heat capacity of the wall.

2.2.2.2. Valves. Inlet and flow valves are considered adiabatic and achieving instantaneous steady state. The inlet valve, *iv*, is described using mass, energy and flow equations:

$$\dot{m}_2 = \dot{m}_1 \tag{10}$$

$$u_2 + \frac{p_2}{\rho_2} = u_1 + \frac{p_1}{\rho_1} \tag{11}$$

$$\frac{\dot{m}_2}{\rho_N} = \frac{514}{3.6 \times 10^5} k_{v,iv} \sqrt{\frac{p_1(p_2 - p_1)}{\rho_N T_2}} \tag{12}$$

$$p_2 = p_2(T_2, \rho_2) \tag{13}$$

$$u_2 = u_2(T_2, \rho_2) \tag{14}$$

The flow control valve, *fv*, is described by the same set of equations than the inlet valve, the only difference between them is that the flow valve is allowed to change its opening fraction along the filling process, $0 \leq x_{fv} \leq 1$, while the inlet valve is completely open during the refueling process:

$$\dot{m}_6 = \dot{m}_5 \tag{15}$$

$$u_6 + \frac{p_6}{\rho_6} = u_5 + \frac{p_5}{\rho_5} \tag{16}$$

$$\frac{\dot{m}_6}{\rho_N} = \frac{514}{3.6 \times 10^5} k_{v,fv} x_{fv} \sqrt{\frac{p_5(p_6 - p_5)}{\rho_N T_5}} \tag{17}$$

$$p_5 = p_5(T_5, \rho_5) \tag{18}$$

$$u_5 = u_5(T_5, \rho_5) \tag{19}$$

$$p_6 = p_6(T_6, \rho_6) \tag{20}$$

$$u_6 = u_6(T_6, \rho_6) \tag{21}$$

2.2.2.3. *Cooler*. Eqs. (22)–(24) describe mass, thermal and pressure dynamics in the cooler, assuming instantaneous steady state in it:

$$\dot{m}_4 = \dot{m}_3 \tag{22}$$

$$u_4 + \frac{p_4}{\rho_4} + q_c = u_3 + \frac{p_3}{\rho_3} \tag{23}$$

$$p_4 = p_3 + \Delta p_c \tag{24}$$

where q_c is the heat transferred per unit mass of hydrogen, and Δp_c is the pressure drop in the cooler, which in this work is assumed to be 0.

2.2.2.4. *Pipe segments*. Mass and energy balances, as well as the hydraulic equations for segments 5–4, Eqs. (25) to (27), and 3-2, Eqs. (28)–(30) reads,

$$\dot{m}_5 = \dot{m}_4 \tag{25}$$

$$u_5 + \frac{p_5}{\rho_5} + q_{54} = u_4 + \frac{p_4}{\rho_4} \tag{26}$$

$$p_5 = p_4 + \Delta p_{54} \tag{27}$$

$$\dot{m}_3 = \dot{m}_2 \tag{28}$$

$$u_3 + \frac{p_3}{\rho_3} + q_{32} = u_2 + \frac{p_2}{\rho_2} \tag{29}$$

$$p_3 = p_2 + \Delta p_{32} \tag{30}$$

Table 1 – Vehicle tank wall properties [8].

Thermophysical		Geometry	
h_{wi} (kW m^{-2} K^{-1})	0.06	V_0 (m^3)	0.12
h_{wo} (kW m^{-2} K^{-1})	0.006	V_w (m^3)	0.0576
ρ_w (kg m^{-3})	1550	A_{wi} (m^2)	2.34
c_w (kJ kg^{-1} K^{-1})	1.374	A_{wi} (m^2)	2.88

The adiabatic and no pressure drop assumptions impose that q_{54}, q_{32}, Δp_{54}, and Δp_{32} are equal to 0.

2.2.2.5. *Thermophysical properties and tank geometry*. All thermodynamic properties of hydrogen are calculated from a high accuracy Helmholtz energy equation [30]. Vehicle tank wall properties are shown in Table 1.

2.3. SAE J2601 protocol

J2601 is a hydrogen fueling protocol for light duty vehicles adopted by the Society of Automotive Engineers (SAE) [29]. The most important variables associated with this filling protocol are the initial vehicle tank pressure and temperature, the ambient temperature, and the dispenser category of the refueling station, defined by the pressure interval and temperature at which it delivers hydrogen into the vehicle tank. From this information, the protocol defines a pressure ramp rate to attain the maximum SOC, within the pressure and temperature limits that ensure mechanical integrity of the tank. The lookup table with the relevant information for the SAE J2601 can be found elsewhere [21]. SAE J2601 also defines a constraint on variations of the fuel delivery temperature using the definition of Rolling Mass Average Fuel Delivery Temperature, to avoid changes larger than 10 °C in the hydrogen dispenser [31]. Although the protocol describes fueling behavior under several different categories of hydrogen delivery temperature and pressure, in this paper the case studies are restricted to the H70-T40 dispenser.

Hydrogen vessels can be classified into four types. While vessels of Types I and II are not designed for vehicular use due to gravimetric capacity and internal corrosion, Types III and IV use lighter materials with working pressure levels up to 35 MPa or 70 MPa respectively, depending on vehicle configuration [18]. Type III (metallic liner with polymeric laminate) and Type IV (thermoplastic liner with polymeric laminate) have the advantage of having higher gravimetric capacity when compared to Types I and II [18,32]. In contrast to Type III, vessels of Type IV have shown higher performance in terms of cyclic internal pressure/temperature, but a higher hydrogen permeation [32]. Types III and IV have different rise and final filling temperatures as a result of their distinct thermal properties [7,18,32]. Both vessels of Types III and IV are considered in the SAE J2601 protocol for refueling light duty vehicles [31].

2.4. Entropy production minimization

In this work, the thermodynamic analyses focuses on the irreversibililty of the refueling operation quantified by the entropy production obtained from the entropy balance equation [33].

The total entropy production of the refueling process $S_{irr}(t_f)$ is computed from the total entropy production of each component of the system,

$$S_{irr}(t_f) = \sum_{k \in \mathcal{K}} \int_0^{t_f} \left(\frac{dS}{dt}\right)_{irr,k} dt, \quad \mathcal{K} = \{0, w, iv, fv\} \tag{31}$$

where $(dS/dt)_{irr,k}$ is the instantaneous entropy production rate of component k, corresponding to: the gas in the vehicle tank (Eq. (32)), the vehicle tank wall (Eq. (33)), the inlet and the flow control valves (Eq. (34) - (35)).

$$\left(\frac{dS}{dt}\right)_{irr,0} = \frac{h_{w0}A_{w0}(T_0 - T_w)}{T_w} + V_0\left(s_0 - s_1 - \frac{p_0}{\rho_0 T_0}\right)\frac{d\rho_0}{dt} + \frac{V_0\rho_0}{T_0}\frac{du_0}{dt} \tag{32}$$

$$\left(\frac{dS}{dt}\right)_{irr,w} = \frac{h_{w,\delta}A_w(T_w - T_\infty)}{T_w} - \frac{h_{w0}A_w(T_0 - T_w)}{T_w} + \frac{\rho_w V_w c_w}{T_w}\frac{dT_w}{dt} \tag{33}$$

$$\left(\frac{dS}{dt}\right)_{irr,iv} = \dot{m}_1 s_1 - \dot{m}_2 s_2 \tag{34}$$

$$\left(\frac{dS}{dt}\right)_{irr,fv} = \dot{m}_3 s_3 - \dot{m}_4 s_4 \tag{35}$$

Note that irreversibilities associated with pipe segments 5–4 and 3–2 are zero due to adiabatic flow and no pressure drop assumptions.

Given the representation of the entire refueling system using a first-principles model, it can be seen that there are two variables that can be used as degrees of freedom: the opening fraction of the flow control valve, x_{fv}, and the cooler heat transferred per unit mass of hydrogen, q_c. Using these manipulated variables, it is possible to formulate an optimal control problem to minimize total entropy production. After incorporating constraints on the manipulated variables and on desired states, the following problem is obtained:

$$\min_{x_{fv}, q_c} \quad S_{irr}(t_f) \tag{36}$$

s.t.

System model (Eqs (1) - (30))

$$T_0(t) \leq T_{max} \tag{37}$$

$$T_{min} \leq T_3(t) \tag{38}$$

$$0 \leq \dot{m}_4(t) \leq \dot{m}_{max} \tag{39}$$

$$SOC_{min} \leq SOC(t_f) \tag{40}$$

$$0 \leq x_{fv}(t) \leq 1 \tag{41}$$

$$q_{min} \leq q_c(t) \leq q_{max} \tag{42}$$

where the objective function, Eq. (36), represents the accumulated entropy production during the refueling process, computed from Eq. (31). Equality path constraints correspond to the model equations derived in Section 2.2.2. Inequality path constraints impose restrictions over the temperature limits for hydrogen in the vehicle tank, Eq. (37), and for the cooler outlet temperature, Eq. (38), as well as on the maximum hydrogen mass flow rate available from the flow control valve, Eq. (39). The state of charge at the end of the filling process is constrained by a minimum desired value in Eq. (40). Lastly, the manipulated variables are constrained due to the limits of equipment as given by Eqs. (41)-(42)

2.5. *Model implementation and solution*

The model was implemented in Python 3.9 using the Pyomo modeling language [34,35]. The optimization problem was converted from continuous to discrete time using pyomo-dae [36]. More specifically, a Lagrange-Radau collocation scheme has been used, with 100 finite elements and two collocation points per element. Finally, the resulting problem was solved using CONOPT4.

The problem size was equal to 23,898 variables and 23,495 equality constraints. Solution time was usually between 30 and 40 s in a Windows 10 environment, using an Intel® Core™ i7-9700 CPU 3.00 GHz processor and 16 GB of RAM memory.

3. Results

3.1. *Model validation*

Fig. 2 shows the outcome of the model derived in Section 2.2.2 using the experimental data reported in Ref. [29]. The model inputs in the validation (Fig. 2a) correspond to pressure, mass flow rate and temperature at the tank inlet measured in *Test* 5-1 A [29]. The model outputs (Fig. 2b) correspond to the SOC and hydrogen temperature in the tank.

Overall, model predictions are in good agreement with experimental data. The predicted and measured SOC discrepancy is less than 1% along the filling process, while maximum hydrogen temperature mismatch is around 7%. During the first 50 s the temperature profile predicted by the model overlaps the measured temperature, from 50 to 300 s the model underpredicts the hydrogen temperature in the tank with a maximum discrepancy of 5.7 °C (7%), and from 300 s to the end of the process overpredicts up to 5.2 °C (7%) the hydrogen temperature in the tank. Experiment-model temperature discrepancies obtained in this work are close to the temperature differences reported using rigorous CFD models (3–7 °C) [37,38] and represent a good trade-off between accuracy and computational cost, taking into account that the model derived in this contribution is typically solved in less than 1 min (30–40 s) while CFD models take hours or days to converge to a solution.

3.2. *Optimal control*

After validation, the model was used to assess the performance of the SAE J2601 benchmark in comparison with an optimal control strategy. The simulations consider a nominal

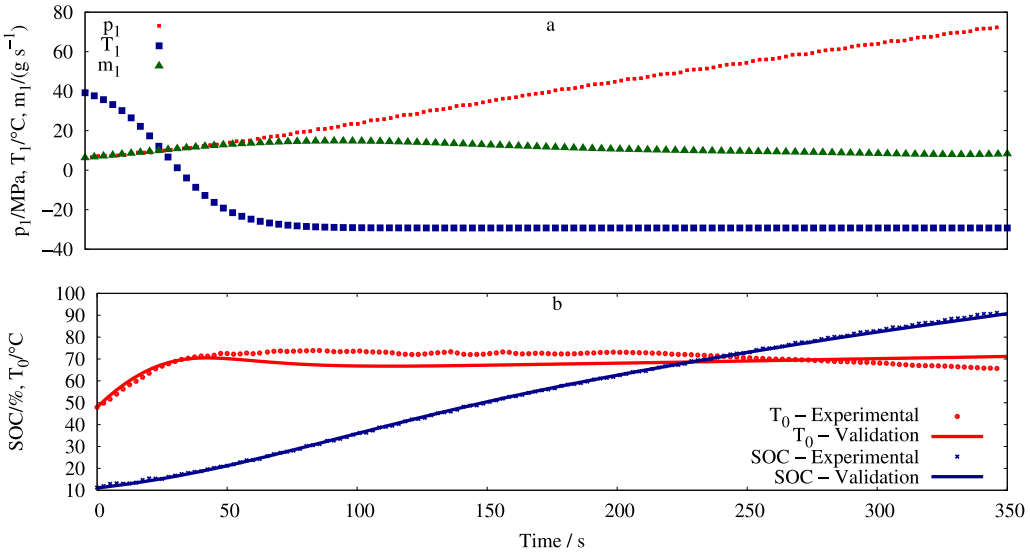

Fig. 2 – Model validation. a. Model inputs: Measured tank inlet pressure (p_1). Measured tank inlet temperature (T_1). Measured tank inlet mass flow rate (m_1). b. Model outputs: State of charge (SOC). Hydrogen temperature in the tank (T_0).

plant model without disturbances. For this reason, it is possible to optimize the whole trajectory of the variables at once, instead of resorting to a moving-horizon strategy such as Model Predictive Control (MPC).

According to the SAE J2601 protocol, the increase of pressure inside the tank must follow a straight line, with slope defined through a lookup table as a function of external temperature, system operating pressure and tank initial state. The temperature after the cooler is kept at −40 °C. On the other hand, the optimal control strategy can manipulate the opening of the flow control valve and the cooler load in order to achieve its objective, i.e., minimum total entropy production after filling the tank. It is significant to stress that the proposed case study (H70-T40) is meant as one illustrative example and not a thorough investigation of all possible combinations of temperature and pressure. The goal of this simulation study is to show how a dynamic optimization can improve process efficiency over a fueling schedule with predefined rules.

In the present case study, it is considered the situation of refilling a tank with an initial pressure of 5 MPa up to 81 MPa under an external temperature of 40 °C. The corresponding value of the Average Pressure Ramp Rate (APRR) given by SAE J2601 is equal to 11.5 MPa/min, which roughly translates into a filling time of 400 s. Therefore, this was the value used as simulation horizon for both strategies. After this definition, the simulation under the protocol was run to determine the final SOC of the system as calculated by the model, which was equal to 99.1%. This value was then used as a terminal constraint on the SOC variable during the optimization (SOC_{min}). Other constraints are imposed accordingly to values in Table 2.

Comparing the profiles of the manipulated variables, the inlet flow rate in Fig. 3 shows that the optimal controller delays the peak of hydrogen injection to around 60 s, in comparison with around 20 s with the protocol. This behavior is associated with lower entropy production in the flow control valve. Regarding the cooler heat transfer in Fig. 3, the actuation of the optimal controller is much less intense, taking advantage of the possibility of keeping the tank temperature at its upper bound (Fig. 5). Moreover, the cooling effort of the optimal controller is milder than the SAE J2601 protocol because it is not required to keep the outlet temperature at −40 °C all the time, leading to a more efficient process in terms of energy expenditure and consequently also operating cost. More precisely, the optimal controller demands only 4.9 MJ, while the protocol uses 6.75 MJ, saving 27% of the total energy consumption.

In respect of temperature profiles, it is important to notice that in all points the process is systematically kept at a higher temperature under the optimal control strategy, as a consequence of the lower cooler loads, but without violating the maximum temperature constraint, Eq. (37), as it can be seen in Fig. 5. The effect is less pronounced in the wall temperature profile, because this variable is more influenced by the values of the heat transfer coefficients.

The evolution of the SOC (Fig. 4) can be analyzed as a consequence of the problem constraints and the trajectory of the flow rate. The initial condition is obviously the same in both cases and the final value is enforced to be the same

Table 2 – Constraints on manipulated variables and states.

Parameter	Value
T_{max} (K)	353.15
T_{min} (K)	233.15
q_{max} (kJ kg^{-1})	0
q_{min} (kJ kg^{-1})	−5000
$\dot{m}_{max}$ (kg s^{-1})	0.06

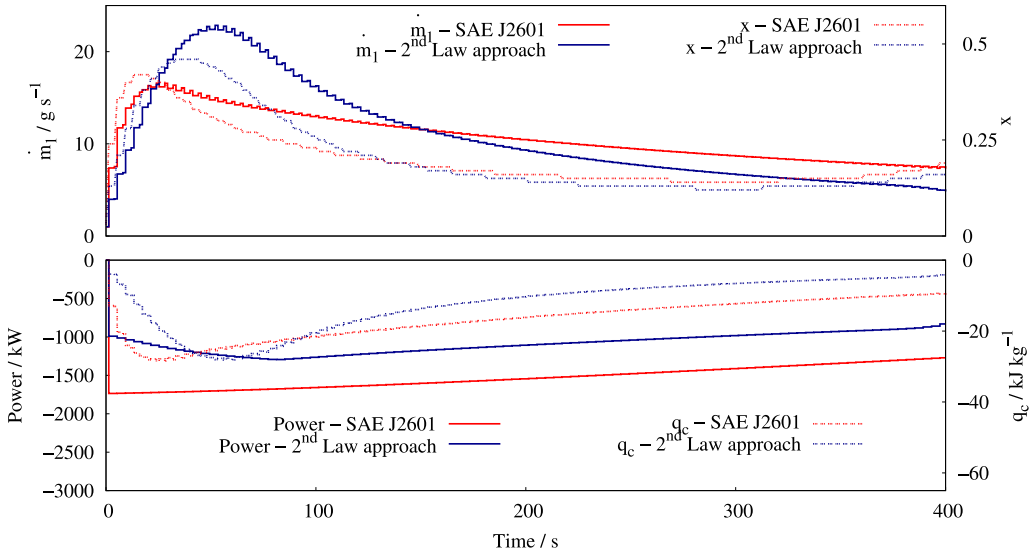

Fig. 3 – Manipulated variables. Dispensed hydrogen mass flow rate ($\dot{m}_1$). Flow valve opening fraction (x). Cooler specific heat load (q_c).

through constraint Eq. (40). Although the SOC is greater at the beginning of the filling process under the protocol due to the larger value of the flow rate, there is a reverse of situation around 40 s. Afterwards, the optimal controller limits the inflow in order to achieve its target at the required time. It is worthwhile to mention that in this work there was no attempt to minimize filling time, but rather to follow the guidelines of SAE J2601.

Lastly, the proposed approach achieves a reduction of around 6.5% in terms of total generated entropy (26.2 vs 28 kJ/K with the protocol). The main responsible for entropy production is the flow control valve, corresponding to more than 85% of the total entropy. In terms of savings, it is the origin of 1.6 kJ/K and the point where the largest reduction in entropy generation happens, which is also roughly 85% of the total savings. A similar behavior is observed at the tank, where entropy production is reduced by 0.4 kJ/K (10%) while this equipment explains roughly 12% of the total entropy generation. However, the same proportionality does not hold for inlet valve, the smallest contributor to the total entropy: under the optimal controller, it actually generates 0.1 kJ/K (50%) more than with the protocol SAE J2601.

The results described in the previous paragraph agree with the observation that in optimally controlled systems the entropy production attempts to be evenly distributed along all components of the system, provided the system has enough degrees of freedom [33]. In this particular case, the two degrees of freedom of the system led to a substantial reduction in the overall entropy production by increasing entropy production in the inlet valve.

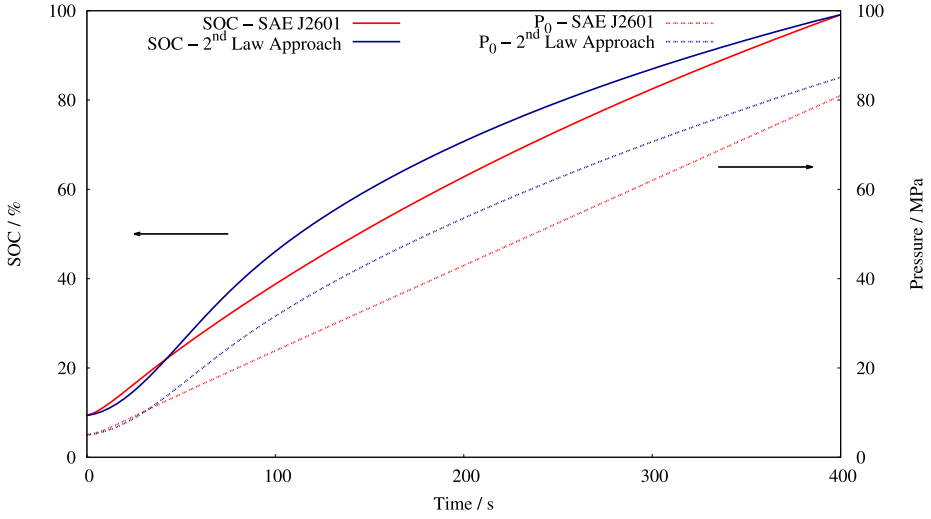

Fig. 4 – Vehicle tank state of charge (SOC) and pressure (p_0).

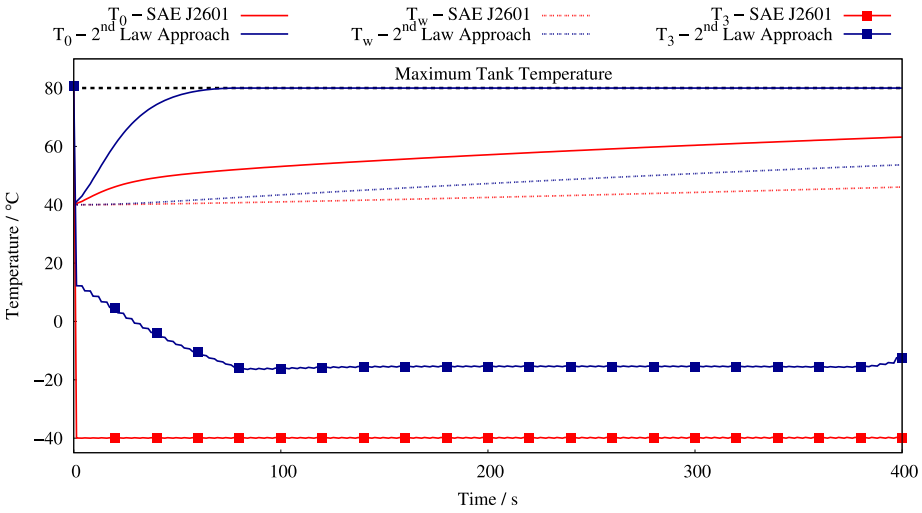

Fig. 5 – Temperature profiles. Hydrogen temperature in the tank (T_0). Tank wall temperature (T_w). Cooler outlet temperature (T_3).

A key difference between the SAE J2601 protocol and the proposed approach is that the fixed APRR dictated by the protocol does not allow enough freedom to the flow control valve to regulate the hydrogen supply, especially at the beginning of the operation where the irreversibility related to pressure drop is the highest (Fig. 6). Additionally, the cooler temperature profile found in the proposed approach, diminished the irreversibility in the tank supplying a stream as close as possible to the tank temperature, in contrast to the SAE J2601 protocol where this value is fixed to −40 °C (Fig. 5).

3.3. *Sensitivity*

In the simulations of Section 3.2, the plant is assumed to behave exactly accordingly to the proposed model, which could induce a bias towards the nominal optimal controller. To alleviate this issue, a sensitivity analysis has been conducted, altering the values of some parameters that are either dependent on the actual design, such as $k_{v,fv}$, or that are subject to more uncertainty, such as h_{wi} and h_{wo}. It was also studied the effect of the external temperature, in order to verify the claim that optimization schemes tend to be more efficient than the protocol SAE J2601 at higher temperatures [21]. The results of these simulations are presented in Table 3.

Regarding the value of the flow coefficient of the flow control valve $k_{v,fv}$, the general behavior is slightly more efficient operation in entropy and energy terms with larger valves, but the obtained gains in simulations are not significant to make any difference in a practical application. However, it is known that if the valve is oversized, the effect of smaller moves are disproportionately large in terms of flow, causing difficulties to keep a safe operation under disturbances. Hence, the conclusion about such parameter is that its sizing can be done purely on the basis of standard process

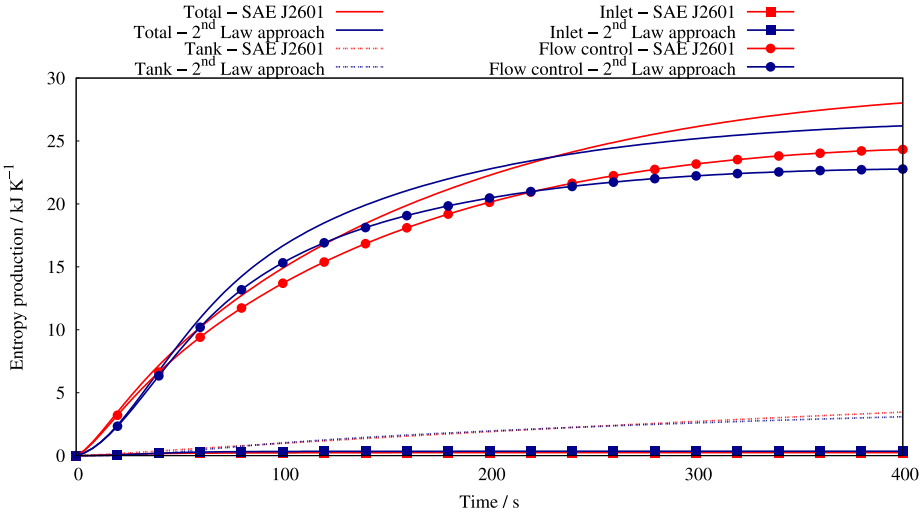

Fig. 6 – Entropy production profiles for SAE J2601 protocol and for Second law approach.

Table 3 – Sensitivity results.

T_∞	k_v	h_{wi}	h_{w0}	Protocol			Min S_{irr} (t_f)			Reduction (Prot - Min S_{irr} (t_f))/Prot	
				SOC(t_f) (%)	S_{irr} (t_f) (kJ/K)	E (t_f) (MJ)	SOC(t_f) (%)	S_{irr} (t_f) (kJ/K)	E (t_f) (MJ)	S_{irr} (t_f)	E (t_f)
40	0.03	60	6	99.1	28.0	6.75	99.1	26.2	4.93	6%	27%
	0.05	60	6	99.1	28.0	6.75	99.1	26.2	4.93	6%	27%
	0.06	60	6	99.1	28.0	6.75	99.1	26.2	4.92	7%	27%
	0.07	60	6	99.1	28.0	6.75	99.1	26.2	4.92	7%	27%
	0.06	55	6	99.0	28.0	6.74	99.0	26.3	5.03	6%	25%
	0.06	65	6	99.2	28.0	6.76	99.2	26.1	4.82	7%	29%
	0.06	60	5	99.1	28.0	6.75	99.1	26.2	4.92	7%	27%
	0.06	60	7	99.1	28.0	6.75	99.1	26.2	4.92	7%	27%
25	0.05	60	6	99.6	27.9	6.76	99.6	26.3	5.07	6%	25%
	0.06	60	6	99.6	27.9	6.76	99.6	26.3	5.05	6%	25%
	0.07	60	6	99.6	27.9	6.76	99.6	26.3	5.04	6%	25%
	0.06	55	6	99.5	27.9	6.74	99.5	26.3	5.16	6%	23%
	0.06	65	6	99.8	27.9	6.77	99.8	26.2	4.95	6%	27%
	0.06	60	7	99.6	27.9	6.76	99.6	26.3	5.05	6%	25%
	0.06	60	5	99.6	27.9	6.76	99.6	26.3	5.05	6%	25%
10	0.05	60	6	99.8	27.7	6.72	99.8	26.3	5.31	5%	21%
	0.06	60	6	99.8	27.7	6.72	99.8	26.3	5.28	5%	21%
	0.07	60	6	99.8	27.7	6.72	99.8	26.3	5.26	5%	22%
	0.06	55	6	99.6	27.7	6.71	99.6	26.4	5.37	5%	20%
	0.06	65	6	100	27.8	6.73	100	26.3	5.16	5%	23%
	0.06	60	7	99.8	27.7	6.72	99.8	26.3	5.28	5%	21%
	0.06	60	5	99.8	27.7	6.72	99.8	26.3	5.28	5%	21%

control analysis, disregarding thermodynamic efficiency considerations.

For both heat transfer coefficients h_{wi} and h_{w0}, the higher the coefficient, the lower entropy production and energy consumption. The effect was found to be almost negligible for h_{w0}, but for the internal coefficient, energy expenditure may decrease up to 4% when the coefficient increases from 60 to 70 kW m^{-2} K^{-1}.

Comparing both approaches, the general picture is that the proposed approach outperforms the protocol SAE J2601 despite the variation in nominal conditions. The size of the effect is influenced by external temperature however, with larger gains for the proposed approach both in terms of entropy and energy at 40 °C than at 25 °C or 10 °C. The reduction goes from around 7% in terms of entropy and 27% in terms of energy at higher temperature to 5% and 20%, respectively, at cooler conditions.

3.4. *Theoretical limit*

To further assess the scale of improvements that can be obtained by replacing the protocol SAE J2601 with an optimal control strategy, in this section the base case study is modified by making it closer to a reversible process, thus finding a lower bound to entropy production in practice. In this theoretical scenario, there is no pressure drop at any points of system. A representation of this situation can be achieved by removing the valve equations of the model, Eqs. (12) and (17), and by assuming that the supply pressure p_6 can be continually adjusted to match the tank pressure p_0.

In a real application, pressure drop at the valves is smaller with larger valve sizing, but excessively increasing their size is undesirable both from economic and process control viewpoints. Moreover, adjustments of the inlet pressure can be achieved if there are multiple tanks of fresh hydrogen at different pressures. However, with a finite number of tanks, it is not possible to regulate p_6 to any desired value, which is the main source of deviation between the proposed theoretical limit and a real setup.

Assuming therefore that there are infinite reservoir tanks and that the valves are large enough, the comparison of Section 3.2 has been revisited as shown in Figs. 7–10. The general shapes of the profiles are the same as before, with the entropy production minimizing strategy delaying the maximal flow rate at the beginning of the filling process in comparison with the protocol SAE J2601. As in Section 3.2, the maximum flow rate is greater than the one achieved by the benchmark protocol, around 20 g s^{-1}, which is still comfortably lower than the admissible upper bound for this variable.

In terms of temperatures, Fig. 9 is also similar to the previously discussed pattern of Fig. 5, with the proposed second law approach allowing for larger tank temperatures since it is able to deviate from the delivery temperature requirement defined by SAE J2601. Since there is no entropy production at the valves under the near-reversible simulated conditions, the only possibility for entropy production reduction is related to the tank. The lower spread between delivery and tank temperatures with the proposed approach justifies that the proposed optimal control strategy is able to reduce total entropy production by 24%, from 3.47 to 2.62 kJ K^{-1}, in comparison with protocol SAE J2601. The entropy production reduction in the tank is almost twice as large in the near-reversible situation than it was in Section 3.2 (3.45–3.09 kJ K^{-1}, respectively). One possible reason for this increased gain is that the

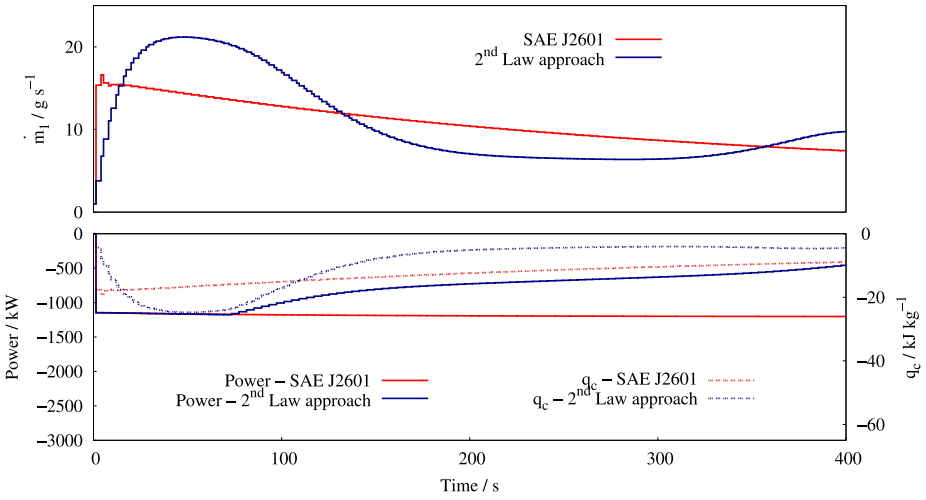

Fig. 7 – Near-reversible scenario: SAE J2601 protocol vs Second law approach. Manipulated variables: Dispensed hydrogen mass flow rate ($\dot{m}_1$). Flow valve opening fraction (x). Cooler specific heat load (q_c).

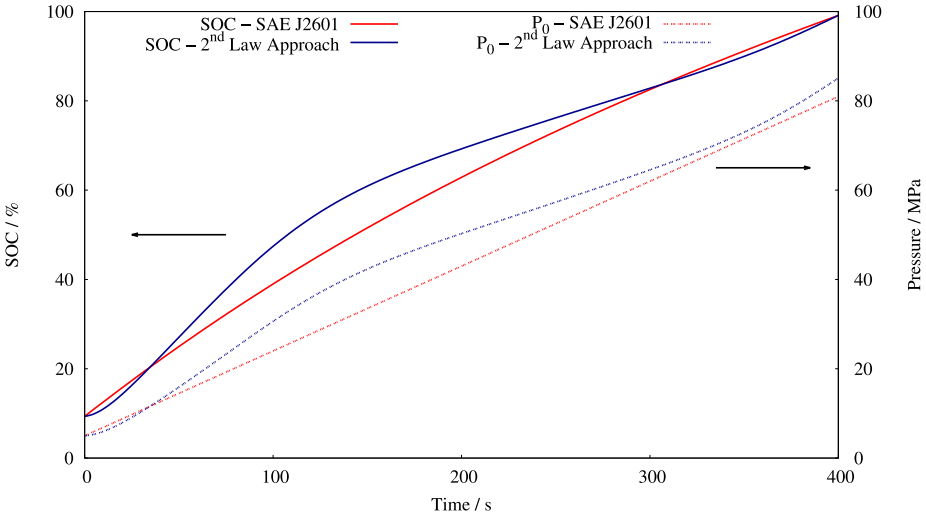

Fig. 8 – Near-reversible scenario: SAE J2601 protocol vs Second law approach. Vehicle tank state of charge (SOC) and pressure (p_0).

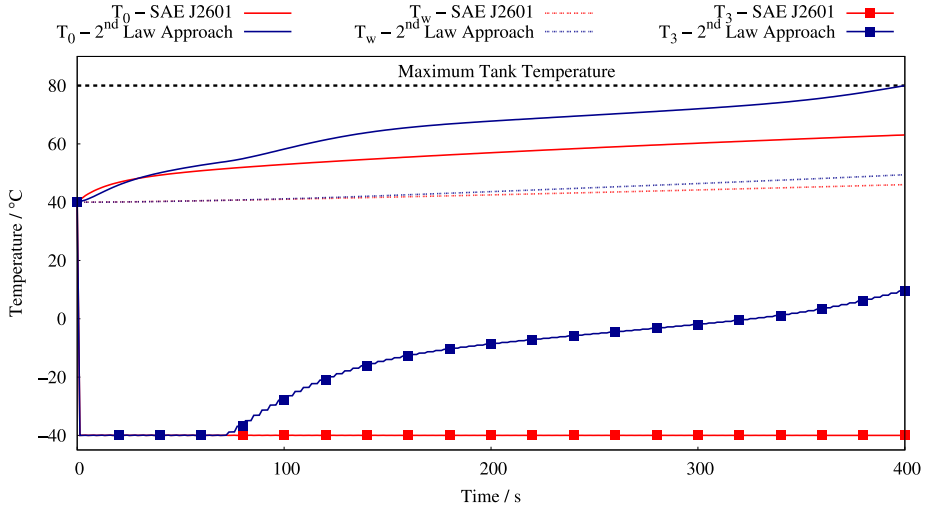

Fig. 9 – Near-reversible scenario: SAE J2601 protocol vs Second law approach. Hydrogen temperature in the tank (T_0). Tank wall temperature (T_w). Cooler outlet temperature (T_3).

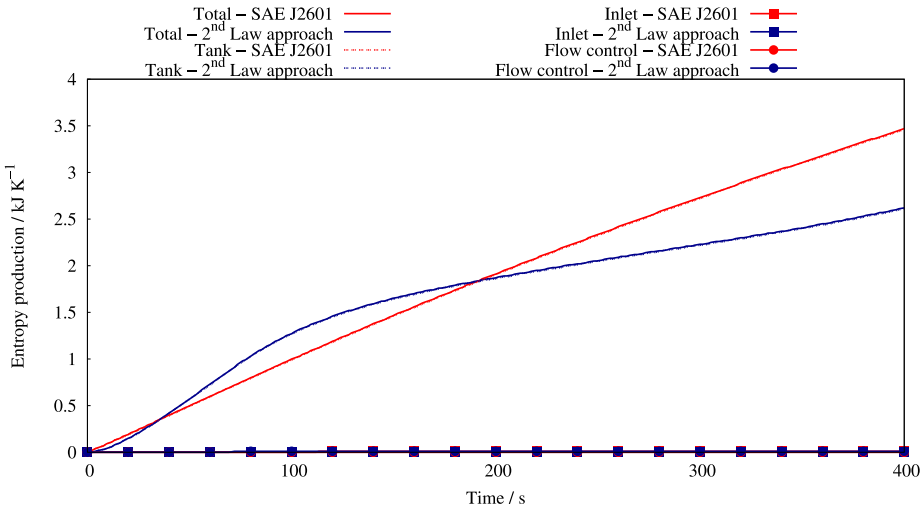

Fig. 10 – Near-reversible scenario: SAE J2601 protocol vs Second law approach. Entropy production profiles.

optimizer can solely focus at the tank entropy production dynamics, while in the previous simulation it was more advantageous to use the control effort to achieve savings in relation to the flow control valve. A similar reduction (24%) can also be seen in terms of total energy expenditure, from 5.11 to 3.86 MJ.

Comparing the results of the proposed controller at this hypothetical conditions and the more practical ones of Section 3.1, it can be seen that total entropy production was reduced by almost 90%, reinforcing that the flow control valve is the main responsible for irreversibilities in practice. In terms of energy, the change is smaller (approximately 43%) but very significant, specially if translated to the actual cost of the process. These findings raise an important question of finding optimal economic configurations for the design of filling stations: although the presence of multiple hydrogen sources and larger valve sizing would demand larger capital investments, they allow for smaller operational expenditure, characterizing a trade-off that is not trivially analyzed without a proper mathematical model.

4. Conclusions and future works

This contribution has addressed the modeling and thermodynamic optimization of an hydrogen refueling station, using a first principles model and the minimization of the entropy production, with the purpose of obtaining insights on the energy efficiency of the SAE J2601 protocol and on possible thermodynamic improvements based solely on operational conditions.

The refueling station model derived in this work was aimed at capturing the main thermodynamic features of the filling process with a relative low computational cost. In this regard, the model showed good agreement with the experimental data with maximum deviation of 1% in the SOC prediction and 7% in the temperature profile along the filling process, while the model solution and optimization took 40 s on average for all the assessed scenarios. The accuracy and solution time exhibited by the model makes it good candidate for finding energy efficient refueling protocols in real-time and for advanced control strategies.

The refueling strategy based on entropy production minimization showed better energy performance than the one proposed by the SAE J2601 protocol, reducing total entropy production by 7% and the heat load in the cooler about 27%. The energy savings obtained by the entropy minimization followed a path of variable pressure ramp and cooler outlet temperatures above −40 °C, contrary to the fixed pressure ramp and cooler outlet temperature defined by the protocol benchmark.

Sensitivity analysis was conducted to evaluate the influence of the flow coefficient of the control valve and heat transfer coefficients. In the first case, optimization results show that the potential entropy production and energy gains with the proposed approach are robust to variations in $k_{v,fv}$, h_{w0}, and h_{wi}. External temperature plays a very significant role and under cooler conditions (25 or 10 °C) energy savings using the proposed approach may decrease to around 20%.

The thermodynamic (near-reversible) limit proposed for the refueling station showed opportunities for significant improvements in energy efficiency, about 43%, when irreversibilities associated to pressure drop in the valves are tackled. In this sense it is of practical interest to determine the optimal pressure cascade for a finite number of hydrogen supply tanks and filling time minimization, topics that will be addressed in future contributions. Future works could explore different configurations, such as other types of tanks and changing the type of fuel dispenser in terms of hydrogen temperature and pressure.

Declaration of competing interest

The authors declare that they have no known competing financial interests or personal relationships that could have appeared to influence the work reported in this paper.

REFERENCES

[1] Bartolucci L, Cordiner S, Mulone V, Pasquale S. Hydrogen based Multi Energy Systems: assessment of the marginal utility of increasing hydrogen penetration on system performances. Int J Hydrogen Energy 2021;46(78):38588–602.

[2] Bahou S. Techno-economic assessment of a hydrogen refuelling station powered by an on-grid photovoltaic solar system: a case study in Morocco. Int J Hydrogen Energy 2023;48(61):23363–72.

[3] Genovese M, Blekhman D, Dray M, Fragiacomo P. Hydrogen station in situ back-to-back fueling data for design and modeling. J Clean Prod 2021;329:129737.

[4] Genovese M, Blekhman D, Dray M, Fragiacomo P. Multi-year energy performance data for an electrolysis-based hydrogen refueling station. Int J Hydrogen Energy 2023. In Press.

[5] Tanç B, Arat H, Baltacioglu E, Aydin K. Overview of the next quarter century vision of hydrogen fuel cell electric vehicles. Int J Hydrogen Energy 2019;44:10120–8. https://doi.org/10.1016/j.ijhydene.2018.10.112.

[6] Greene D, Ogden J, lin Z. Challenges in the designing, planning and deployment of hydrogen refueling infrastructure for fuel cell electric vehicles. eTransportation 2020;6. https://doi.org/10.1016/j.etran.2020.100086.

[7] Genovese M, Fragiacomo P. Hydrogen refueling station: overview of the technological status and research enhancement. J Energy Storage 2023;61:106758. https://doi.org/10.1016/j.est.2023.106758.

[8] Olmos F, Manousiouthakis VI. Hydrogen car fill-up process modeling and simulation. Int J Hydrogen Energy 2013;38:3401–18. https://doi.org/10.1016/j.ijhydene.2012.12.064.

[9] Olmos F, Manousiouthakis VI. Gas tank fill-up in globally minimum time: theory and application to hydrogen. Int J Hydrogen Energy 2014;39(23):12138–57. https://doi.org/10.1016/j.ijhydene.2014.05.091.

[10] Ruffio E, Saury D, Petit D. Thermodynamic analysis of hydrogen tank filling. Effects of heat losses and filling rate optimization. Int J Hydrogen Energy 2014;39(24):12701–14. https://doi.org/10.1016/j.ijhydene.2014.06.069.

[11] Bourgeois T, Brachmann T, Barth F, Ammouri F, Baraldi D, Melideo D, et al. Optimization of hydrogen vehicle refuelling requirements. Int J Hydrogen Energy 2017;42(19):13789–809. https://doi.org/10.1016/j.ijhydene.2017.01.165.

[12] Rothuizen E, Mérida W, Rokni M, Wistoft-Ibsen M. Optimization of hydrogen vehicle refueling via dynamic simulation. Int J Hydrogen Energy 2013;38(11):4221–31. https://doi.org/10.1016/j.ijhydene.2013.01.161.

[13] Rothuizen E, Rokni M. Optimization of the overall energy consumption in cascade fueling stations for hydrogen vehicles. Int J Hydrogen Energy 2014;39(1):582–92. https://doi.org/10.1016/j.ijhydene.2013.10.066.

[14] Caponi R, Ferrario AM, Bocci E, Bødker S, del Zotto L. Single-tank storage versus multi-tank cascade system in hydrogen refueling stations for fuel cell buses. Int J Hydrogen Energy 2022;47(64):27633–45. https://doi.org/10.1016/j.ijhydene.2022.06.100.

[15] Farzaneh-Gord M, Deymi-Dashtebayaz M, Rahbari HR, Niazmand H. Effects of storage types and conditions on compressed hydrogen fuelling stations performance. Int J Hydrogen Energy 2012;37(4):3500–9. https://doi.org/10.1016/j.ijhydene.2011.11.017.

[16] Wu Y, Geng X, Chen J, Shao S. Impact of pipelines on cooling demand in the gaseous hydrogen refueling station. Int J Hydrogen Energy 2023;48(26):24412–25. https://doi.org/10.1016/j.ijhydene.2023.03.168.

[17] Tian Z, Lv H, Zhou W, Zhang C, He P. Review on equipment configuration and operation process optimization of hydrogen refueling station. Int J Hydrogen Energy 2022;47(5):3033–53. https://doi.org/10.1016/j.ijhydene.2021.10.238.

[18] Li M, Bai Y, Zhang C, Song Y, Jiang S, Grouset D, et al. Review on the research of hydrogen storage system fast refueling in fuel cell vehicle. Int J Hydrogen Energy 2019;44(21):10677–93. https://doi.org/10.1016/j.ijhydene.2019.02.208.

[19] James W. An introduction to SAE hydrogen fueling standardization. US Department of Energy; 2014.

[20] Genovese M, Cigolotti V, Jannelli E, Fragiacomo P. Hydrogen refueling process: theory, modeling, and in-force applications. Energies 2023;16(6):2890. https://doi.org/10.3390/en16062890.

[21] Reddi K, Elgowainy A, Rustagi N, Gupta E. Impact of hydrogen SAE J2601 fueling methods on fueling time of light-duty fuel cell electric vehicles. Int J Hydrogen Energy 2017;42(26):16675–85. https://doi.org/10.1016/j.ijhydene.2017.04.233.

[22] Deng S, Li F, Luo H, Yang T, Ye F, Chahine R, et al. Lumped parameter modeling of SAE J2601 hydrogen fueling tests. Sustainability 2023;15(2):1448. https://doi.org/10.3390/su15021448.

[23] Chochlidakis CG, Rothuizen ED. Overall efficiency comparison between the fueling methods of SAE J2601 using dynamic simulations. Int J Hydrogen Energy 2020;45(20):11842–54. https://doi.org/10.1016/j.ijhydene.2020.02.068.

[24] Bai Y, Zhang C, Duan H, Jiang S, Zhou Z, Grouset D, et al. Modeling and optimal control of fast filling process of hydrogen to fuel cell vehicle. J Energy Storage 2021;35:102306. https://doi.org/10.1016/j.est.2021.102306.

[25] Monde M, Woodfield P, Takanato T, Kosaka M. Estimation of temperature change in practical hydrogen pressure tanks being filled at high pressures of 35 and 70 MPa. Int J Hydrogen Energy 2012;37:5723–34. https://doi.org/10.1016/j.ijhydene.2011.12.136.

[26] Melideo D, Baraldi D, De Miguel Echavarria D, Acosta Iborra B. Effects on some key-parameters on the thermal stratification in hydrogen tanks during the filling process. Int J Hydrogen Energy 2019;44:13569–82. https://doi.org/10.1016/j.ijhydene.2019.03.187.

[27] Bourgeois T, Ammouri F, Baraldi D, Moretto P. The temperature evolution in compressed gas filling process: a review. Int J Hydrogen Energy 2018;43:2268–92. https://doi.org/10.1016/j.ijhydene.2017.11.068.

[28] Immel R, Mack-Gardner A. Development and validation of a numerical thermal simulation model for compressed hydrogen gas storage tanks. SAE Int J Engine 2011;4(1):1850–61. https://www.jstor.org/stable/26278263.

[29] Schneider J, Meadows G, Mathison SR, Veenstra MJ, Shim J, Wistoft-Ibsen Immel MR, et al. Validation and sensitivity studies for SAE J2601, the light duty vehicle hydrogen fueling standard. SAE Int J Alt Power 2014;3:257–309. https://www.jstor.org/stable/26169058.

[30] Leachman JW, Jacobsen RT, Penoncello SG, Lemmon EW. Fundamental equations of state for parahydrogen, normal hydrogen, and orthohydrogen. J Phys Chem Ref Data 2009;38:721–48. https://doi.org/10.1063/1.3160306.

[31] of Automotive Engineers S. Fueling protocols for light duty gaseous hydrogen surface vehicles. SAE International; 2020.

[32] Blanco-Aguilera R, Martinez-Agirre M, Berasategi J, Penalba M, Bou-Ali MM, Shevtsova V. Effect of liner thermal properties and liner pre-cooling on the thermal management of fast-filling of hydrogen tanks. Int J Hydrogen Energy 2023. In press.

[33] Kjelstrup S, Bedeaux D, Johannessen E, Gross J. Non-equilibrium thermodynamics for engineers. World Scientific; 2010.
[34] Bynum ML, Hackebeil GA, Hart WE, Laird CD, Nicholson BL, Siirola JD, et al. Pyomo—optimization modeling in python. vol. 67. 3rd ed. Springer Science & Business Media; 2021.
[35] Hart WE, Watson JP, Woodruff DL. Pyomo: modeling and solving mathematical programs in Python. Mathematical Programming Computation 2011;3(3):219–60. https://doi.org/10.1007/s12532-011-0026-8.
[36] Nicholson B, Siirola JD, Watson JP, Zavala VM, Biegler LT. pyomo.dae: a modeling and automatic discretization framework for optimization with differential and algebraic equations. Mathematical Programming Computation 2018;10(2):187–223. https://doi.org/10.1007/s12532-017-0127-0.
[37] Melideo D, Baraldi D, Acosta Iborra B, Ortiz Cebolla R, Moretto P. CFD simulations of filling and emptying of hydrogen tanks. Int J Hydrogen Energy 2017;42:7304–13. https://doi.org/10.1016/j.ijhydene.2016.05.262.
[38] Zhao B, Wei H, Peng X, Feng J, Jia X. Experimental and numerical research on temperature evolution during the fast-filling process of a type III hydrogen tank. Energies 2022;15:3811. https://doi.org/10.3390/en15103811.